INSTITUTE OF PHYSICS PUBLISHING JOURNAL OF PHYSICS: CONDENSED MATTER

J. Phys.: Condens. Matter **15** (2003) S3411–S3420 PII: S0953-8984(03)66420-9

Capillary condensation of colloid–polymer mixtures confined between parallel plates

Matthias Schmidt[1], **Andrea Fortini and Marjolein Dijkstra**

Soft Condensed Matter, Debye Institute, Utrecht University, Princetonplein 5, 3584 CC Utrecht, The Netherlands

Received 21 July 2003
Published 20 November 2003
Online at stacks.iop.org/JPhysCM/15/S3411

Abstract

We investigate the fluid–fluid demixing phase transition of the Asakura–Oosawa model colloid–polymer mixture confined between two smooth parallel hard walls using density functional theory and computer simulations. Comparing fluid density profiles for statepoints away from colloidal gas–liquid coexistence yields good agreement of the theoretical results with simulation data. Theoretical and simulation results predict consistently a shift of the demixing binodal and the critical point towards higher polymer reservoir packing fraction and towards higher colloid fugacities upon decreasing the plate separation distance. This implies capillary condensation of the colloid liquid phase, which should be experimentally observable inside slitlike micropores in contact with a bulk colloidal gas.

1. Introduction

Capillary condensation denotes the phenomenon that spatial confinement can stabilize a liquid phase coexisting with its vapour in bulk [1, 2]. In order for this to happen the attractive interaction between the confining walls and the fluid particles needs to be sufficiently strong. Although the main body of work on this subject has been done in the context of confined simple liquids, one might expect that capillary condensation is particularly well suited to be studied with colloidal dispersions. In these complex fluids length scales are on the micron rather than on the ångström scale which is typical for atomic substances. Attraction between colloidal particles can be generated and precisely tuned by adding non-adsorbing polymer. The presence of the polymers induces an effective attraction between the colloids that may lead to fluid–fluid phase separation reminiscent of the gas–liquid transition in atomic systems: the phase that is poor in colloids corresponds to the gas and the phase that is dense in colloids corresponds to the liquid [3].

[1] On leave from Institut für Theoretische Physik II, Heinrich-Heine-Universität Düsseldorf, Universitätsstraße 1, D-40225 Düsseldorf, Germany.

0953-8984/03/483411+10$30.00

A particularly simple model to study colloid–polymer mixtures is that proposed by Asakura and Oosawa (AO) [4] and Vrij [5], where colloids are represented as hard spheres and polymers as effective, overlapping spheres that cannot penetrate the colloids. Indeed this model displays stable gas and liquid phases and also a crystalline solid [6–12].

The same mechanism that generates an effective attraction between two colloidal particles via depletion of polymers gives also rise to attraction between a single colloidal particle and a simple hard wall leading to strong adsorption of colloids at the wall [13]. Close to the gas branch of the demixing binodal the hard wall is wet by the colloidal liquid, purely driven by entropy, and an intriguing scenario of entropic wetting with a finite sequence of layering transitions in the partial wetting regime was found with density functional theory (DFT) [14, 15] and computer simulations [11], and recently also in a rod–sphere mixture [16]. In fact, there is also experimental evidence for wetting of a smooth hard substrate by the colloid-rich phase [17–19]. Less attention has been paid to the influence of strong confinement on colloid–polymer mixtures, exceptions being exposure to a standing laser field [20] and immersion into random sphere matrices acting as porous media [21, 22].

In this work we investigate the effect of contact with two narrowly spaced, parallel smooth hard walls. We use Monte Carlo (MC) computer simulation and DFT to investigate a range of wall separation distances from ten down to one colloid diameter—covering the dimensional crossover to two remaining space coordinates. Both theory and simulation treat the polymers explicitly, and hence include, in principle, all polymer-induced many-body interactions between colloids. Testing the theory for a case of strong confinement by comparing colloid and polymer density profiles away from coexistence with simulation data demonstrates good accuracy. From theory and simulation results for fluid–fluid coexistence we find that indeed confinement stabilizes the colloidal liquid inside the capillary, hence capillary condensation does occur. These findings should be experimentally observable in colloid–polymer mixtures prepared such that the colloidal bulk gas is in contact with a thin slit pore, and the adsorption inside the pore is measured.

The paper is organized as follows. In section 2 we define the AO model between parallel walls explicitly. In section 3 both the MC and DFT techniques are presented. Section 4 discusses results for one-body density profiles and the demixing phase diagram. We conclude in section 5.

2. Model

The AO model is a binary mixture of colloidal hard spheres (species c) of diameter σ_c and of spheres representing polymer coils (species p) with diameter σ_p [4, 5]. The pair interaction between colloids is that of hard spheres: $V_{cc}(r) = \infty$ if $r < \sigma_c$ and zero otherwise, where r is the separation distance between particle centres. The interaction between a colloid and a polymer is also that of hard spheres: $V_{cp}(r) = \infty$ if $r < (\sigma_c + \sigma_p)/2$ and zero otherwise. The polymers, however, are assumed to be ideal, hence the polymer–polymer interaction vanishes for all distances, $V_{pp}(r) = 0$. To model the confinement between smooth parallel hard walls we consider external potentials acting on species $i = c, p$, given by

$$V_{\mathrm{ext},i}(z) = \begin{cases} 0 & \sigma_i/2 < z < H - (\sigma_i/2) \\ \infty & \text{otherwise,} \end{cases} \tag{1}$$

where z is the spatial coordinate normal to the walls, and H is the wall separation distance; see figure 1 for an illustration of the situation.

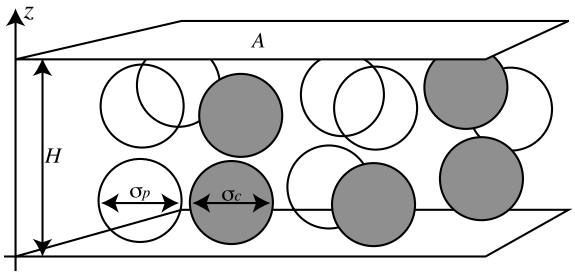

Figure 1. Illustration of the AO model of hard sphere colloids (grey circles) of diameter σ_c and ideal polymers (transparent circles) of diameter σ_p confined between parallel hard walls of area A and separation distance H. Colloids behave as hard spheres, polymers cannot penetrate colloids, and polymers may freely overlap. The walls are impenetrable to both components. The z-axis is perpendicular to the walls, and the origin is located at the lower wall.

The size ratio $q = \sigma_p/\sigma_c$ is a geometric control parameter; the ratio H/σ_c rules the strength of the confinement. We denote the packing fractions by $\eta_i = \pi\sigma_i^3 N_i/(6AH)$, where N_i is the number of particles of species i and A is the lateral (normal to the z-direction) area of the system. As alternative thermodynamic parameters, we use the packing fraction in a pure reservoir of polymers, η_p^r, and the fugacity of the colloids, z_c.

3. Methods

3.1. Computer simulations

We employ Gibbs ensemble MC simulations, where phase coexistence is directly accessible through the use of two simulation boxes, each representing one of the coexisting states [23, 24]. Both boxes contain the confining walls at fixed plate separation distance H. Let $N_{i,a}$ be the number of particles of species i in box $a = 1, 2$, and $A_a H$ be the volume of box a, where A_a is its lateral area. Then $A_1 H + A_2 H =$ constant and $N_{i,1} + N_{i,2} =$ constant, while fluctuations of $N_{i,a}$ and A_a inside each individual box $a = 1, 2$ are allowed. Thus three different (randomly chosen) types of MC move are performed: single-particle moves of colloids and polymers inside each simulation box, moves that transfer particles from one box to the other to ensure equal chemical potential, and volume exchanges between both boxes to ensure equal wall–fluid interfacial tension via rescaling the lateral box dimensions (and the x- and y-components of particle positions) while keeping the plate separation distance H (and the z-components of all particle positions) constant. We start from a random, non-overlapping configuration, and use 10^8 MC moves for equilibration and typically 3×10^8 production moves for each pair of coexistence statepoints. Acceptance ratios for particle exchange depend strongly on statepoint and decrease, upon increasing η_p^r, from about 50% close to the critical point to about 5% for the highest values considered. The coexistence densities are obtained from the maxima of a histogram of the number of particles in each box. Fugacities are calculated via the test particle insertion method [25]. Typical total particle numbers are $N_{c,1} + N_{c,2} =$ 200–400 for colloids and, dependent on the statepoint, $N_{p,1} + N_{p,2} =$ 600–2000 for polymers. The total lateral area of both boxes, $A_1 + A_2$, is between $400\sigma_c^2$ and $2500\sigma_c^2$. Each run was divided into ten blocks and error bars were obtained from one standard deviation of the block averages.

3.2. Density functional theory

The grand potential of the binary mixture is written as a functional of the (inhomogeneous) one-body density distributions $\rho_i(\mathbf{r})$ as

$$\Omega[\rho_c, \rho_p] = k_B T \sum_{i=c,p} \int d\mathbf{r}\, \rho_i [\ln(\rho_i(\mathbf{r})\Lambda_i^3) - 1] + F_{exc}[\rho_c, \rho_p] + \sum_{i=c,p} \int d\mathbf{r}\, \rho_i(\mathbf{r})[V_{ext,i}(\mathbf{r}) - \mu_i], \quad (2)$$

where Λ_i is the thermal wavelength and μ_i is the chemical potential of species i, k_B is Boltzmann's constant and T is temperature. Although equation (2) is general, for the present application we take the external potentials, $V_{ext,i}$, to be those modelling the slit pore, equation (1). The first term on the right-hand side of (2) is the free energy functional of a binary ideal gas; the unknown part in (2) is the (Helmholtz) excess free energy functional, F_{exc}, that describes the influence of interparticle interactions. Here we take the fundamental measures approximation [26] of [9, 10] that is specifically tailored for the AO model. This is a weighted density approximation where F_{exc} is expressed as a spatial integral over an excess free energy density, which depends on a set of weighted densities that are obtained through convolutions of the bare density profiles with geometrically inspired weight functions. Details can be found in [9, 10]. In order to obtain density profiles the minimization conditions,

$$\frac{\delta\Omega}{\delta\rho_i(\mathbf{r})} = 0, \qquad i = c, p, \quad (3)$$

are solved by a standard iteration technique, and the value of the grand potential is obtained by inserting the solutions of (3) into (2). In order to have direct access to phase coexistence we minimize two systems simultaneously and adjust the chemical potentials of both species iteratively such that in the final state both systems possess the same grand potential. This procedure is inspired by the Gibbs ensemble MC method above.

4. Results

In the following we will restrict ourselves to the polymer-to-colloid size ratios $q = 1$. For this value considerable knowledge about bulk [11] and hard wall behaviour [11, 15] is available. Moreover, it is an experimentally readily accessible case.

4.1. Comparison

We start by comparing density profiles for statepoints where we expect the system to be in the one-phase mixed fluid state. As our DFT is known to be accurate in bulk [10], and at single hard planar walls [15], we focus on a case of strong confinement and hence consider $H/\sigma_c = 2$. Figure 2 displays colloid and polymer profiles as a function of the z-coordinate normal to the walls. Both colloid and polymer density profiles are largest at contact with the walls, $z/\sigma_c = 0.5, 1.5$.

The agreement of the theoretical curves with the simulation data is quantitatively good. We note, however, that for still larger values of η_p^r differences begin to emerge (results not shown). As such conditions get close to the demixing transition, we attribute this to the differences in the results for the demixing binodal.

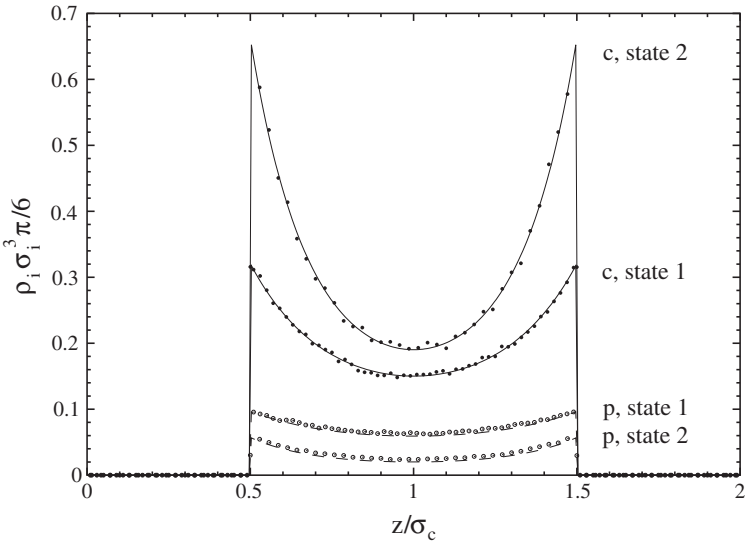

Figure 2. Density profiles $\rho_i(z)\sigma_i^3\pi/6$, $i = \mathrm{c}, \mathrm{p}$ as a function of the coordinate z/σ_c normal to the plates for plate separation distance $H/\sigma_\mathrm{c} = 2$. Results from DFT (curves) and MC (symbols) are shown for $\eta_\mathrm{c} = 0.0997$, $\eta_\mathrm{p}^\mathrm{r} = 0.266$ (statepoint 1) and $\eta_\mathrm{c} = 0.157$, $\eta_\mathrm{p}^\mathrm{r} = 0.367$ (statepoint 2).

4.2. Phase diagram

For large enough concentration of polymer, phase separation into colloid-poor gas and colloid-rich liquid is expected to occur in our model capillary. As an illustration we display snapshots of a pair of coexisting states in figure 3 for large wall separation distance $H/\sigma_\mathrm{c} = 10$. In the gas phase, there is a significant number of colloids located close to the wall, and density profiles (not shown) indicate strong adsorption of colloids at both walls in the capillary gas. This is due to the polymer-induced depletion attraction between colloid particle and wall. The capillary liquid is dense in colloids and polymers tend to build clusters of overlapping particles.

We have simulated many such coexisting states for varying densities and values of H/σ_c. The resulting set of phase diagrams is depicted in figure 4, where colloid packing fraction, η_c, and polymer reservoir packing fraction, $\eta_\mathrm{p}^\mathrm{r}$, are taken as independent parameters. The binodals possess a lower (in $\eta_\mathrm{p}^\mathrm{r}$) critical point, and a rapidly increasing density jump upon increasing $\eta_\mathrm{p}^\mathrm{r}$. The shape of the binodal is similar to that of the liquid–gas transition in simple fluids upon identifying $\eta_\mathrm{p}^\mathrm{r}$ with inverse temperature.

Upon increasing confinement via decreasing H/σ_c, the critical point moves significantly upwards to higher $\eta_\mathrm{p}^\mathrm{r}$, again similar to the common trend of capillary-induced decrease of critical temperature. The theoretical binodals agree well with the simulation data, except for a slight overestimation of the coexisting liquid density, and a quite prominent underestimation of $\eta_\mathrm{p}^\mathrm{r}$ at the critical point. The trend that the simulation result for the critical point is at higher $\eta_\mathrm{p}^\mathrm{r}$ than in theory is already known in bulk [11], which we can confirm here. Decreasing H, the deviation gets stronger, and for $H/\sigma_\mathrm{c} = 2$ quite strong deviations are found. As this is already close to a two-dimensional situation, this finding is in accordance with the expectation that the DFT becomes less accurate in the critical region.

Before discussing the ultimate crossover to two dimensions in more detail, we present the same phase diagram in a different representation, namely as a function of colloid chemical potential $\mu_\mathrm{c} = \ln(z_\mathrm{c}\sigma_\mathrm{c}^3)$ and of $\eta_\mathrm{p}^\mathrm{r}$ in figure 5. As a function of these variables, each pair of

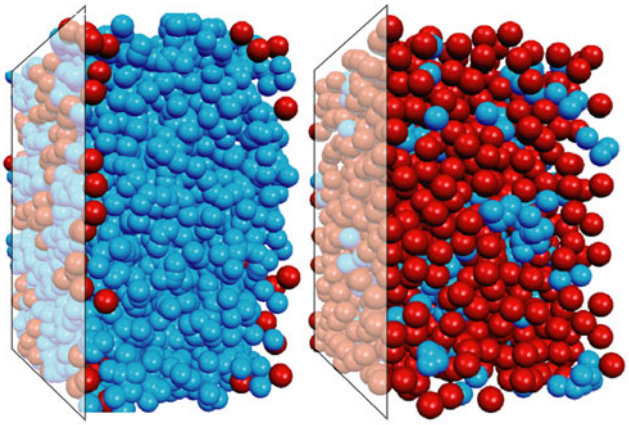

Figure 3. Snapshots from computer simulation of the confined colloidal gas (left) in coexistence with the confined colloidal liquid (right). Colloids (dark red) and polymers (light blue) are immersed between two parallel plates (transparent; only the left-hand wall is shown) with separation distance $H/\sigma_c = 10$ and orientation perpendicular to the horizontal axis. The polymer reservoir packing fraction is $\eta_p^r = 1.116$. Note that compared to figure 1 the system is rotated by 90° around the viewing direction.

(This figure is in colour only in the electronic version)

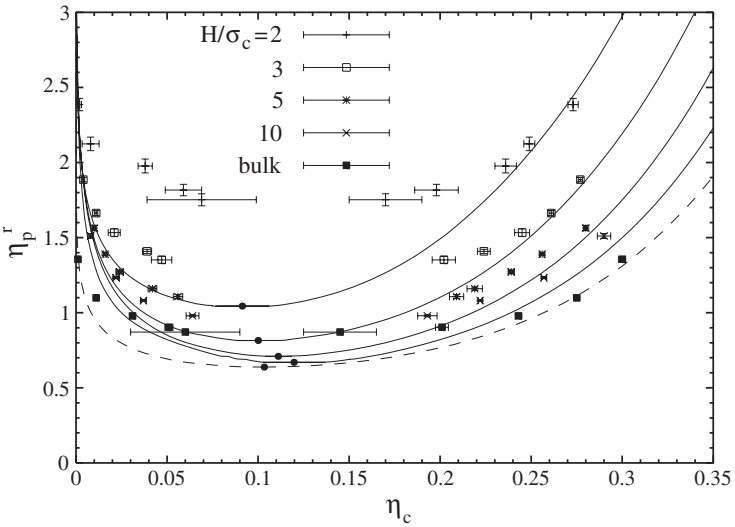

Figure 4. Phase diagram of the AO model between parallel hard walls with separation distance $H/\sigma_c = 2, 3, 5, 10, \infty$ (bulk) as a function of colloid packing fraction in the slit, η_c, and polymer reservoir packing fraction, η_p^r. DFT results for the binodal (curves; from top to bottom for increasing H; the dashed curve indicates the bulk result) and critical point (filled dots) are shown along with MC results for coexisting states (symbols). Coexistence is along horizontal tie lines (not shown).

coexisting phases (gas and liquid phases with different η_c) collapses to a single point as μ_c and η_p^r are equal for the coexisting phases. By reducing H, the critical point and the binodal shifts to larger z_c and larger η_p^r. Consider a statepoint on the gas side of the phase diagram. If this is chosen sufficiently close to the bulk binodal, it might well reside on the liquid side of

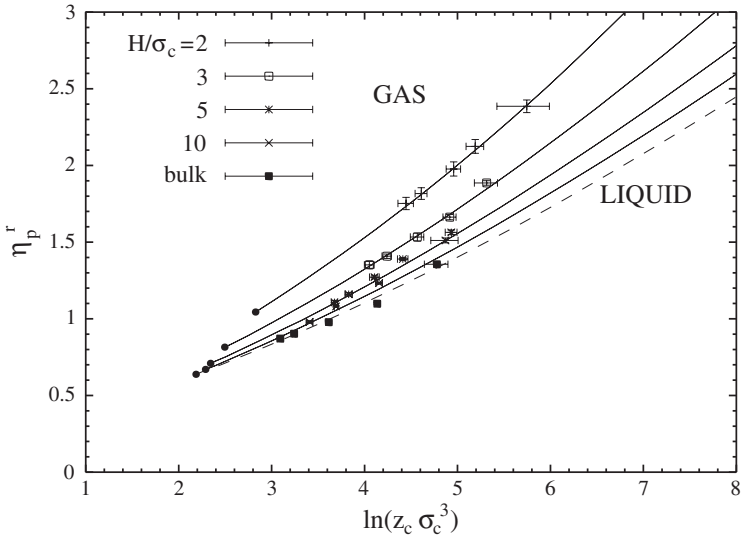

Figure 5. The same as figure 4, but as a function of colloid chemical potential $\ln(z_c\sigma_c^3)$ and of polymer reservoir packing fraction η_p^r. Shown are the results for $H/\sigma_c = 2, 3, 5, 10$ (solid lines and symbols as indicated from top to bottom) and bulk (dashed line and full squares).

the confined system, indicating a liquid phase in the capillary in equilibrium with a bulk gas. Hence this demonstrates the occurrence of capillary condensation in the slit pore. Except for the precise location of the critical point, the overall agreement between DFT and MC results is quite satisfactory.

We have compared these findings to those predicted by the Kelvin equation, generalized to binary mixtures [27][2]. Three statepoints were chosen: $\eta_p^r = 0.84$ in the complete wetting regime, $\eta_p^r = 1.1$ just above the first layering transition [15], and $\eta_p^r = 2$ deep in the partial wetting regime, see figure 6. For the intermediate case the shift in η_p^r and z_c is correctly predicted by the Kelvin equation, even for strong confinement. For high η_p^r there are differences emerging, especially for the cases $H/\sigma_c = 2, 3$. Close to the critical point, the performance is not very satisfactory, as the growth of wetting layers at the walls is not taken into account.

We have attempted to include results for H very close to σ_c. As can be guessed from the above results for larger H, we find that the values of η_p^r needed to induce phase separation become increasingly large and no longer fit on the same scale. In fact, close to $H/\sigma_c = 1$ this is a trivial effect of dimensional crossover, which we can remedy by using scaled variables. See figure 7 for the binodals in reservoir representation, but as a function of η_c and $\eta_p^r(H - \sigma_c)/H$. The simulation results for the quasi-two-dimensional system are obtained by choosing $H/\sigma_c = 1.01$ (and we have checked the independence from this precise value, by also considering $H/\sigma_c = 1.001$ at one statepoint and finding the same result within the error bars). Indeed, the two-dimensional result is now on the same scale as the results for larger slits. We also show the binodal obtained from the two-dimensional DFT [10], that is equivalent to free volume theory [28] in two dimensions. Again the theory overestimates the

[2] See equations (40) and (41) in [27]. Adapting those to the present case, we obtain the shifts in chemical potentials, $\Delta\mu_i$, of species $i = c, p$ from simultaneous solution of $2(\gamma_{wg} - \gamma_{wl})/(H - \sigma) = \Delta\mu_c\rho_c^l + \Delta\mu_p\rho_p^l$ and $\Delta\mu_p = -\Delta\mu_c\rho_c^g/\rho_p^g$, where ρ_i^l and ρ_i^g are the coexisting densities, γ_{wl} and γ_{wg} are the hard wall interface tensions of the liquid and the gas phase, respectively, and $\sigma \equiv \sigma_c = \sigma_p$ for the present size ratio, $q = 1$.

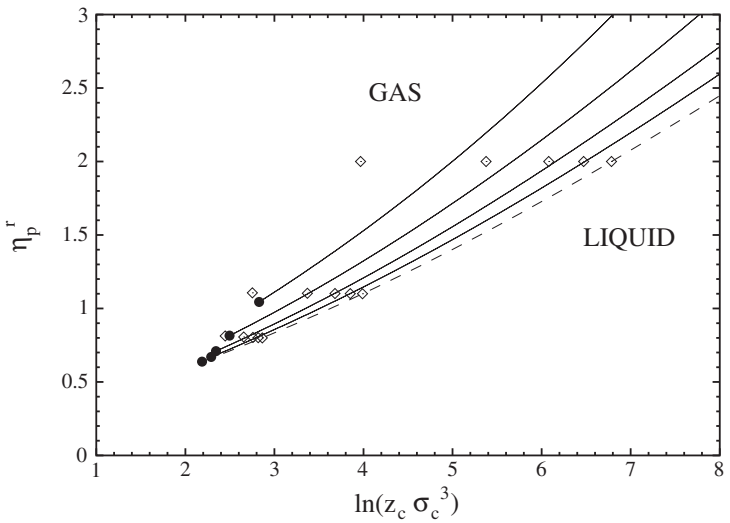

Figure 6. The same as figure 5; shown are the DFT results (curves) along with the predictions from applying the generalized Kelvin equation (open symbols) for statepoints $\eta_p^r = 0.84, 1.1, 2$ and $H/\sigma_c = \infty$ (bulk), 10, 5, 3, 2 (from right to left).

area of demixed states in the phase diagram, somewhat worse than in three dimensions. This probably reflects the difficulty of predicting critical points in two dimensions reliably.

More remarkably, however, is that the scaling leads to an almost complete data collapse of the MC results for *all* slit widths. This is an empirical finding, and we are not aware that such a scaling has been found previously in simple liquids, where one had to relate temperature to confinement in order to have a similar scaling. The binodals from DFT do not collapse as nicely as the MC results; the scaling somewhat overcompensates the shift in η_p^r with decreasing H. Finally, in figure 8 we show the phase diagram as a function of two rescaled variables, i.e. $\eta_p^r(H-\sigma_c)/H$ and $\ln(z_c(H-\sigma_c)/H)$ demonstrating that both fugacities need to be rescaled to obtain the data collapse. However, in this representation the collapse is not as perfect as in figure 7. Note also that the binodal for the 2D case lies on the opposite site of the bulk binodal, as compared to the cases of finite H. This indicates non-monotonic behaviour in the range $1 < \sigma_c/H < 2$. In fact the scaling overcompensates, as the binodals for $2 \leqslant H/\sigma_c \leqslant 10$ are in opposite order compared to figure 5.

5. Conclusions

In conclusion, we have considered a binary mixture of hard sphere colloidal particles and added non-adsorbing polymer modelled by effective spheres in contact with a slit pore of parallel hard walls. We find that this capillary induces stability of a (thin film) liquid phase that coexists with the bulk colloidal gas phase. This behaviour can be understood from the strong depletion attraction between (each) wall and the colloidal particles.

Both treatments, computer simulation and DFT, take into account all induced many-body terms in the polymer-mediated effective interaction between the colloidal spheres. We achieve this by treating, in both cases, the full binary mixture.

As an outlook on possible future work, we mention the interesting problem of freezing in confined systems, and in particular how the pure hard sphere behaviour [29, 30] is changed by adding polymer.

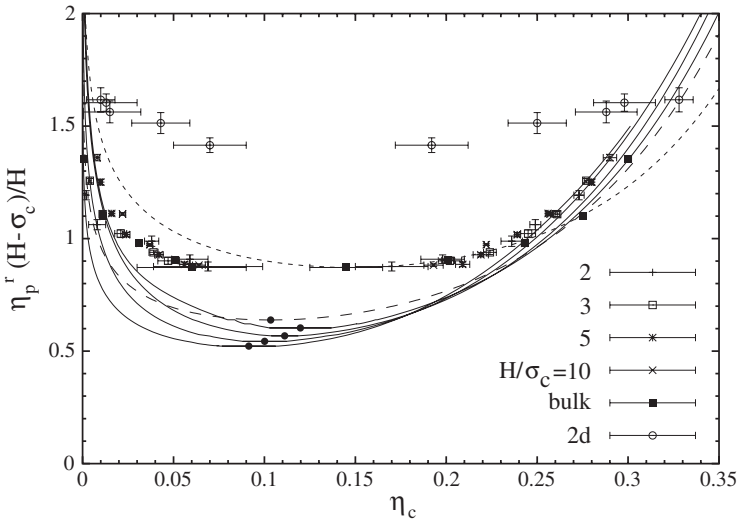

Figure 7. The same as figure 4, but as a function of η_c and the rescaled polymer packing fraction, $\eta_p^r(H-\sigma_c)/H$. Also shown are the results for the two-dimensional (2D) system obtained from simulations for $H/\sigma_c = 1.01$ and free volume theory (short dashed curve).

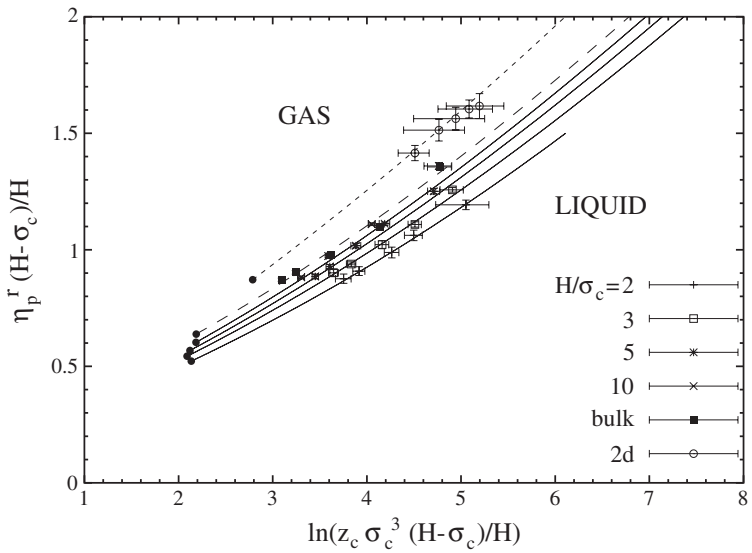

Figure 8. The same as figure 5, but as a function of the rescaled variables $\ln(z_c\sigma_c^3(H-\sigma_c)/H)$ and $\eta_p^r(H-\sigma_c)/H$.

We emphasize that our predictions can, in principle, be experimentally tested with colloid–polymer mixtures confined between two glass walls. In particular, keeping this slit pore in contact with a bulk colloidal gas, very close to coexistence, and monitoring the amount of adsorbed colloid material in the slit should be fruitful.

Acknowledgments

We thank Dirk G A L Aarts, Henk N W Lekkerkerker, and Paul P F Wessels for many useful and inspiring discussions. J M Brader is acknowledged for sending us his surface tension data [15]. This work is part of the research program of the *Stichting voor Fundamenteel Onderzoek der Materie* (FOM), that is financially supported by the *Nederlandse Organisatie voor Wetenschappelijk Onderzoek* (NWO). Support by the DFG SFB TR6 'Physics of colloidal dispersions in external fields' is acknowledged.

References

[1] Evans R 1990 *J. Phys.: Condens. Matter* **2** 8989
[2] Gelb L D, Gubbins K E, Radhakrishnan R and Sliwinska-Bartkowiak M 1999 *Rep. Prog. Phys.* **62** 1573
[3] Poon W C K 2002 *J. Phys.: Condens. Matter* **14** R859
[4] Asakura S and Oosawa F 1954 *J. Chem. Phys.* **22** 1255
[5] Vrij A 1976 *Pure Appl. Chem.* **48** 471
[6] Gast A P, Hall C K and Russell W B 1983 *J. Colloid Int. Sci.* **96** 251
[7] Lekkerkerker H N W, Poon W C K, Pusey P N, Stroobants A and Warren P B 1992 *Europhys. Lett.* **20** 559
[8] Dijkstra M, Brader J M and Evans R 1999 *J. Phys.: Condens. Matter* **11** 10079
[9] Schmidt M, Löwen H, Brader J M and Evans R 2000 *Phys. Rev. Lett.* **85** 1934
[10] Schmidt M, Löwen H, Brader J M and Evans R 2002 *J. Phys.: Condens. Matter* **14** 9353
[11] Dijkstra M and van Roij R 2002 *Phys. Rev. Lett.* **89** 208303
[12] Bolhuis P G, Louis A A and Hansen J P 2002 *Phys. Rev. Lett.* **89** 128302
[13] Brader J M, Dijkstra M and Evans R 2001 *Phys. Rev.* E **63** 041405
[14] Brader J M, Evans R, Schmidt M and Löwen H 2002 *J. Phys.: Condens. Matter* **14** L1
[15] Brader J M 2001 *PhD Thesis* University of Bristol
[16] Roth R, Brader J M and Schmidt M 2003 *Europhys. Lett.* **63** 549
[17] Aarts D G A L, van der Wiel J H and Lekkerkerker H N W 2003 *J. Phys.: Condens. Matter* **15** S245
[18] Aarts D G A L and Lekkerkerker H N W 2003 private communication
[19] Wijting W K, Besseling N A M and Cohen Stuart M A 2003 *Phys. Rev. Lett.* **90** 196101
[20] Götze I O, Brader J M, Schmidt M and Löwen H 2003 *Mol. Phys.* **101** 1651
[21] Schmidt M, Schöll-Paschinger E, Köfinger J and Kahl G 2002 *J. Phys.: Condens. Matter* **14** 12099
[22] Wessels P P F, Schmidt M and Löwen H 2003 unpublished
[23] Panagiotopoulos A Z 1987 *Mol. Phys.* **61** 813
[24] Panagiotopoulos A Z 1987 *Mol. Phys.* **62** 701
[25] Smit B and Frenkel D 1989 *Mol. Phys.* **68** 951
[26] Rosenfeld Y 1989 *Phys. Rev. Lett.* **63** 980
[27] Evans R and Marini Bettolo Marconi U 1987 *J. Chem. Phys.* **86** 7138
[28] Lee J-T and Robert M R 1999 *Phys. Rev.* E **60** 7198
[29] Schmidt M and Löwen H 1996 *Phys. Rev. Lett.* **76** 4552
[30] Schmidt M and Löwen H 1997 *Phys. Rev.* E **55** 7228